Potential energy surface of the CO_2–N_2 van der Waals complex

Sameh Nasri, Yosra Ajili, Nejm-Eddine Jaidane, Yulia N. Kalugina, Philippe Halvick, Thierry Stoecklin, and Majdi Hochlaf'

Citation: J. Chem. Phys. **142**, 174301 (2015); doi: 10.1063/1.4919396
View online: http://dx.doi.org/10.1063/1.4919396
View Table of Contents: http://aip.scitation.org/toc/jcp/142/17
Published by the American Institute of Physics

Potential energy surface of the CO_2–N_2 van der Waals complex

Sameh Nasri,[1,2] Yosra Ajili,[1,2] Nejm-Eddine Jaidane,[1] Yulia N. Kalugina,[3] Philippe Halvick,[4] Thierry Stoecklin,[4] and Majdi Hochlaf[2,a)]

[1]*Laboratoire de Spectroscopie Atomique, Moléculaire et Applications-LSAMA, Université de Tunis El Manar, Tunis, Tunisia*

[2]*Université Paris-Est, Laboratoire Modélisation et Simulation Multi Echelle, MSME UMR 8208 CNRS, 5 bd Descartes, 77454 Marne-la-Vallée, France*

[3]*Department of Optics and Spectroscopy, Tomsk State University, 36 Lenin Ave., Tomsk 634050, Russia*

[4]*Institut des Sciences Moléculaires, Université de Bordeaux, CNRS UMR 5255, 33405 Talence Cedex, France*

(Received 11 February 2015; accepted 17 April 2015; published online 1 May 2015)

Four-dimensional potential energy surface (4D-PES) of the atmospherically relevant CO_2–N_2 van der Waals complex is generated using the explicitly correlated coupled cluster with single, double, and perturbative triple excitation (CCSD(T)-F12) method in conjunction with the augmented correlation consistent triple zeta (aug-cc-pVTZ) basis set. This 4D-PES is mapped along the intermonomer coordinates. An analytic fit of this 4D-PES is performed. Our extensive computations confirm that the most stable form corresponds to a T-shape structure where the nitrogen molecule points towards the carbon atom of CO_2. In addition, we located a second isomer and two transition states in the ground state PES of CO_2–N_2. All of them lay below the $CO_2 + N_2$ dissociation limit. This 4D-PES is flat and strongly anisotropic along the intermonomer coordinates. This results in the possibility of the occurrence of large amplitude motions within the complex, such as the inversion of N_2, as suggested in the recent spectroscopic experiments. Finally, we show that the experimentally established deviations from the C_{2v} structure at equilibrium for the most stable isomer are due to the zero-point out-of-plane vibration correction. © *2015 AIP Publishing LLC.* [http://dx.doi.org/10.1063/1.4919396]

I. INTRODUCTION

van der Waals (vdW) complexes involving CO_2 molecules (CO_2-X, X = He, Ar, Kr, H_2, ...)[1–4] were subject of numerous theoretical and experimental studies given the crucial role of CO_2 in atmospheric, planetary (e.g., Mars and Venus), and environmental media and in a large panel of industrial applications (such as in agrobusiness, pharmacy, biochemistry, and material sciences, where it mainly replaces treatments using hazardous liquids). In the atmosphere, CO_2 possesses, for instance, the ability to absorb infrared (IR) light which overlaps with the thermal emission of Earth leading hence to the global atmospheric warming. The complexation of CO_2 to other gases affects the frequencies of the IR active CO_2 modes resulting in a better overlap with the Earth's emission. More interestingly, the totally symmetric modes of isolated CO_2, which are IR transparent, become weakly allowed upon complexation and therefore contribute to the greenhouse effect. From a fundamental point of view, CO_2–X complexes are prototype systems for studying characteristics of intermolecular interactions and molecular dynamics of weakly bound complexes.

N_2 is the most abundant gas in the Earth's atmosphere and CO_2 represents the fourth most abundant gas in dry atmosphere. The formation of CO_2–N_2 weakly bound complex in these media was suggested and discussed more than once in the literature. In 1988, Walsh *et al.*[5] measured the rotationally resolved spectrum of this complex in the asymmetric stretch region of the CO_2 monomer by diode laser absorption spectroscopy of a pulsed molecular beam. They deduced a T-shaped structure for CO_2–N_2, with O=C=O as the cross of the T and the N≡N axis pointing toward the carbon atom in good accordance with the nuclear spin statistics and rotational constants deduced from their spectra. Ten years later, Gomez Castano *et al.*[6] confirmed the results of Walsh *et al.* using a matrix isolation Fourier Transform IR (FTIR) spectroscopy. In 2010, Frohman *et al.*[7] provided the microwave spectrum of CO_2–N_2 and of its isotopomers using a pulsed-jet Fourier transform microwave (FTMW) spectrometer. More recently, Konno *et al.*[8] recorded a high-resolution infrared spectrum of $^{12}C^{18}O_2$–$^{14}N_2$ isotopologue seeded in a pulsed molecular beam using a diode laser absorption spectroscopy. They covered the spectral region in the vicinity of the ν_3 band (2314 cm^{-1}) of isolated $^{12}C^{18}O_2$. All these experimental works confirmed the earlier findings of Walsh *et al.* Theoretically, the most stable form of CO_2–N_2 complex has been characterized at the MP2/aug-cc-pVDZ,[6] MP2/6-311 + G(d),[9] CCSD(T)/aug-cc-pVXZ (X = D, T, Q, 5, 6, Complete Basis Set (CBS)), and CCSD(T)-F12(a/b)/cc-pVXZ-F12 (X = D, T, Q)[10] levels of theory, and the ground potential energy surface (PES) has been explored using fixed monomer geometries using the MP4 and CCSD(T)[11] methods. Again, these theoretical works showed that the experimentally determined structure of Walsh *et al.* is the most stable isomer of CO_2–N_2. In addition, the bonding within this complex is interpreted by a Natural Bond Orbital (NBO) analysis in terms of "donor–acceptor" interactions, where molecular nitrogen acts as electron donor and the carbon dioxide plays the role of electron acceptor.

a)Author to whom correspondence should be addressed. Electronic mail: hochlaf@univ-mlv.fr

In a series of papers, we showed that the CCSD(T)-F12/augmented correlation consistent triple zeta (aug-cc-pVTZ) explicitly correlated method is accurate enough to describe correctly the regions of the vdW intermolecular interactions, which are sensitive to electron correlation. We established also that this level of theory is suited to generate accurate multidimensional PESs of weakly bound dimers with reduced computational cost.[12–17] At present, we take advantage of this technique to derive the 4D-PES of the CO_2–N_2 complex along the intermonomer coordinates. Later on, we deduced an analytical representation of this 4D-PES. Our results confirm the occurrence of large amplitude motions within this complex as suggested after the analysis of the microwave (μ w) spectrum of Frohman *et al.*[7]

II. ELECTRONIC STRUCTURE COMPUTATIONS

Previous theoretical computations dealing with the CO_2–N_2 complex proved that its electronic wavefunction is dominantly described by a unique electron configuration. For such monoconfigurational molecular systems, Coupled Cluster (CC) methods are the most appropriate for accounting for electron correlation. Therefore, we will discuss in the following only the results issued from CC computations.

For electronic structure computations, we used the MOLPRO (version 2012.1) suite of programs.[18] In all calculations, the correction of basis set superposition error (BSSE) of Boys and Bernardi[19] was taken into account in the description of the interaction potential

$$V(R,\theta_1,\theta_2,\varphi) = E_{CO_2N_2}(R,\theta_1,\theta_2,\varphi) - E_{CO_2}(R,\theta_1,\theta_2,\varphi) - E_{N_2}(R,\theta_1,\theta_2,\varphi),$$

where the energies of CO_2 and N_2 are calculated in the full basis set of the complex. The calculations of the 4D-PES were performed using the molecular distances at r(CO) = 2.217 27 a_0 and r(NN) = 2.106 65 a_0 (1 bohr = 1 a_0 = 0.5292 Å). These values are slightly larger than the r_e distances computed for the CO_2–N_2 complex at the CCSD(T)-F12a/aug-cc-pVTZ level of theory (*vide infra*). They correspond to a roughly estimated r_0 structure for this complex allowing closer comparison with experiment.

A. Benchmark calculations: Molecular region

Figure 1 shows the comparison of the interaction potentials for selected angular orientations of CO_2 with respect to N_2. These potentials were calculated using both standard[20,21] and explicitly correlated coupled cluster approaches[22] with and without taking into account the triple corrections for comparison. We used also several basis sets (aug-cc-pVXZ, X = D, T, Q) extrapolated then to the CBS limit following the procedure described by Peterson *et al.*[23] and Feller and Sordo.[24] Within the standard CC computations, the atoms were described using aug-cc-pVTZ basis set.[25,26] For explicitly correlated computations, we followed the methodology established in Refs. 12–17 where the atoms were described by the aug-cc-pVTZ basis set[25,26] and we used the corresponding auxiliary basis sets and density fitting functions[27,28] (i.e., the default CABS(OptRI) basis sets of Peterson and co-workers as implemented in MOLPRO).

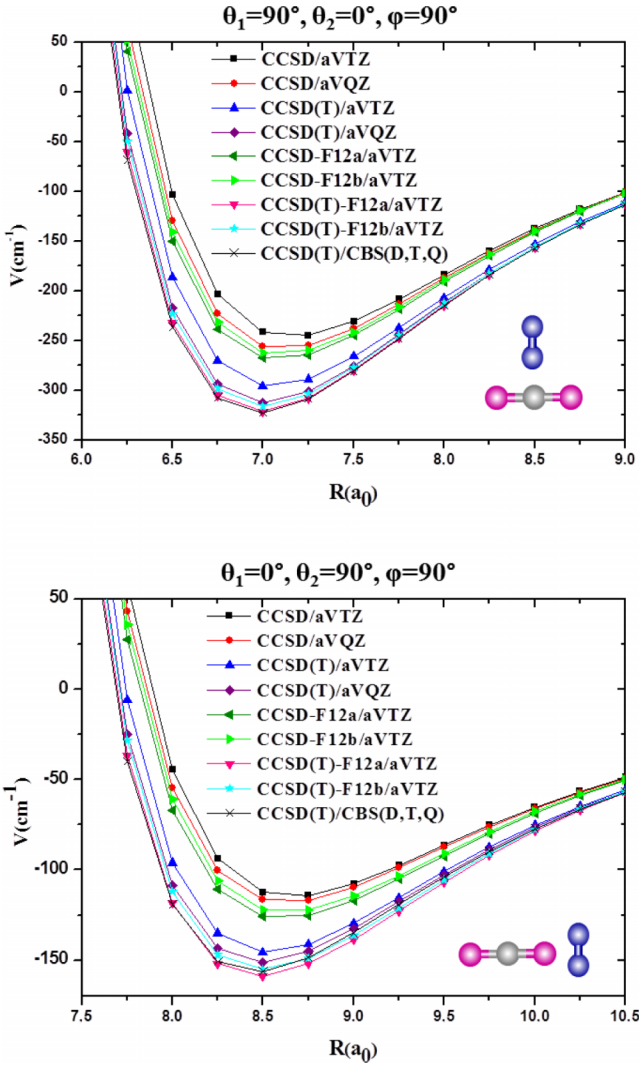

FIG. 1. One-dimensional cuts of 4D-PES for two relative orientations of N_2 with respect to CO_2 computed at different levels of theory.

Figure 1 reveals that the depth of the potential wells increases by increasing the size of the basis set and that those computed without considering the triple correction are less deep than those when this correction is considered. Therefore, one cannot omit the use of triple excitations for the accurate description of this complex. Moreover, Figure 1 reveals that the CCSD(T)-F12a/aug-cc-pVTZ potentials are the closest to those computed at the CCSD(T)/CBS level, which is used here as reference. It is worth noting that CCSD(T)-F12b/aug-cc-pVTZ leads to slightly less deep potentials. Hence, CCSD(T)-F12a/aug-cc-pVTZ provides an excellent description of the interaction energies. In addition, the CPU time and the disk usage for a single point calculation, reported in the supplementary material,[29] confirm the gain of time and computational efforts that this method permits. Consequently, we can be quite confident in the accuracy of the PES obtained using CCSD(T)-F12a/aug-cc-pVTZ. More generally, these findings join the main conclusions we draw through the benchmark studies on CO_2–CO_2[17] and DABCO-Rg (Rg = Rare gas)[14] weakly bound systems.

B. Asymptotic behavior

In order to investigate the long range interaction of the CO_2–N_2 system, we have performed the multipolar expansion[30] of the interaction potential. In this long-range approximation, the interaction energy is expressed as the sum of electrostatic (E_{elec}), induction (E_{ind}), and dispersion (E_{disp}) energies. For the case of rigid linear interacting CO_2 and N_2 molecules, these energies are written as follows:

$$E_{elec} = \frac{1}{9}T_{\alpha\beta\gamma\delta}\Theta^{CO_2}_{\alpha\beta}\Theta^{N_2}_{\gamma\delta} + \frac{1}{315}T_{\alpha\beta\gamma\delta\epsilon\nu}\left[\Theta^{CO_2}_{\alpha\beta}\Phi^{N_2}_{\gamma\delta\epsilon\nu} + \Theta^{N_2}_{\alpha\beta}\Phi^{CO_2}_{\gamma\delta\epsilon\nu}\right], \quad (1)$$

$$E_{ind} = -\frac{1}{18}T_{\alpha\gamma\delta}T_{\beta\epsilon\nu}\left[\alpha^{CO_2}_{\alpha\beta}\Theta^{N_2}_{\gamma\delta}\Theta^{N_2}_{\epsilon\nu} + \alpha^{N_2}_{\alpha\beta}\Theta^{CO_2}_{\gamma\delta}\Theta^{CO_2}_{\epsilon\nu}\right], \quad (2)$$

$$E_{disp} = -\frac{1}{2\pi}\Big[T_{\alpha\beta}T_{\gamma\delta}\int_0^\infty \bar{\alpha}^{CO_2}_{\alpha\gamma}(i\omega)\bar{\alpha}^{N_2}_{\beta\delta}(i\omega)d\omega + \frac{1}{3}T_{\alpha\beta\gamma}T_{\delta\epsilon\nu}\int_0^\infty (\bar{\alpha}^{CO_2}_{\alpha\delta}(i\omega)\bar{C}^{N_2}_{\beta\gamma,\epsilon\nu}(i\omega) + \bar{\alpha}^{N_2}_{\alpha\delta}(i\omega)\bar{C}^{CO_2}_{\beta\gamma,\epsilon\nu}(i\omega))d\omega + \frac{2}{15}T_{\alpha\beta}T_{\gamma\delta\epsilon\nu}\int_0^\infty (\bar{\alpha}^{CO_2}_{\alpha\gamma}(i\omega)\bar{E}^{N_2}_{\beta,\delta\epsilon\nu}(i\omega) + \bar{\alpha}^{N_2}_{\alpha\gamma}(i\omega)\bar{E}^{CO_2}_{\beta,\delta\epsilon\nu}(i\omega))d\omega\Big]. \quad (3)$$

Here, $\alpha = (2\alpha_{xx} + \alpha_{zz})/3$ is a mean polarizability.

In Eqs. (1)–(3), $\alpha_{\alpha\beta}$, $C_{\alpha\beta,\gamma\delta}$, and $E_{\alpha,\beta\gamma\delta}$ are dipole, quadrupole, and dipole-quadrupole polarizabilities of the monomers; $\Theta_{\alpha\beta}$ and $\Phi_{\alpha\beta\gamma\delta}$ are the permanent quadrupole and hexadecapole moments of the monomers; $\bar{\alpha}_{\alpha\beta}$, $\bar{C}_{\alpha\beta,\gamma\delta}$, and $\bar{E}_{\alpha,\beta\gamma\delta}$ denote the imaginary frequency-dependent polarizabilities of the monomers. Tensor $T_{\alpha\beta\ldots\nu} = \nabla_\alpha \cdots \nabla_\nu R^{-1}$ is symmetric in all subscripts and tensor of rank n, T^n is proportional to $R^{-(n+1)}$. If there are repeated subscripts, the T tensor is equal to zero. In Eqs. (1)–(3), there is a summation over the repeated Greek indices. Molecular properties used for computation of multipolar expansion series were calculated at the CCSD(T)/aug-cc-pV5Z level of theory within the finite-field approach of Cohen and Roothaan[41] and presented in Table I along with the available experimental and previous theoretical data. The imaginary frequency-dependent properties for CO_2 and N_2 molecules were computed using the CCSD propagator method (propagators exact up to the fourth order)[42] in aug-cc-pV5Z basis set. The number of frequencies for the numerical integration was set to 100 to ensure the convergence of the dispersion coefficient within 0.01%. The calculations were carried out using Molpro 2012 package.[18] The corresponding results could be found in the supplementary material.[29]

Figure 2 presents the one-dimensional cuts of the interaction potential along the R coordinate obtained at the CCSD(T)-F12a level and analytically via the multipolar expansion (Eqs. (1)-(3)). It is notable that the analytical description of interaction potential for this complex is in very good agreement with the *ab initio* results. This long-range approximation describes well the interaction energy for the configuration that corresponds to the global minimum ($\theta_1 = 90°$, $\theta_2 = 0°$, $\varphi = 0°$, see below) for $R > 10$ a_0, and for the configuration corresponding to the local minimum ($\theta_1 = 0°$, $\theta_2 = 90°$, $\varphi = 0°$, see below) for $R > 9$ a_0. The leading electrostatic term is proportional to the product of quadrupole moments of CO_2 and N_2 molecules and goes as R^{-5}. The leading dispersion interaction varies as R^{-6} and is proportional to the product of polarizabilities of CO_2 and N_2 molecules. We can conclude that the CCSD(T)-F12a/aug-cc-pVTZ method performs very well for selected configurations at long-range separations which confirms again the validity of this methodology.[15,43,17]

III. CO_2–N_2 GROUND STATE INTERACTION POTENTIAL

A. Generation of the 4D-potential energy surface

We showed in Sec. II that CCSD(T)-F12a/aug-cc-pVTZ method allows accurate description, with reduced computational cost, of both long-range and intermediate-range inter-

TABLE I. Electric properties of CO_2 and N_2 monomers calculated at the CCSD(T)/aug-cc-pV5Z level and the literature data.

	CO_2		N_2	
Property	This work	Literature	This work	Literature
Θ_{zz}	−3.15	−3.12 ± 0.18[a] −3.19 ± 0.13[c] −3.19[f]	−1.08	−1.04 ± 0.02[b] −1.13,[d] 1.12[e] −1.09 ± 0.07[g]
Φ_{zzzz}	−2.08	−1.7[f]	−6.81	−6.37[b] −6.75,[d] −6.70[e]
α_{xx}	12.92	12.99[f]	10.33	10.24,[d] 10.35[h]
α_{zz}	27.11	27.07[f]	15.14	14.84,[d] 15.05[h]
α	17.65	17.54 ± 0.93[i] 17.69[f]	11.93	11.77,[d] 11.92[h] 11.74[j]
$C_{xx,xx}$	33.93	34.13[f]	20.20	20.51[d]
$C_{xz,xz}$	53.73	54.81[f]	27.54	27.20[d]
$C_{zz,zz}$	82.26	80.94[f]	34.82	34.64[d]
$E_{x,xxx}$	−68.62	−68.9[f]	−23.01	−23.42,[d] −24.24[e]
$E_{z,zzz}$	190.16	187.6[f]	38.25	39.59,[d] 39.25[e]

[a]From magnetizability anisotropy measurements.[31]
[b]From optical birefringence measurements.[35]
[c]From optical birefringence measurements.[32]
[d]Theoretical calculations from Ref. 36.
[e]Theoretical calculations from Ref. 38.
[f]Theoretical calculations from Ref. 33.
[g]From optical birefringence measurements.[37]
[h]Raman depolarization and reactivity data spectroscopy.[39]
[i]Experimental results from Ref. 34.
[j]Experimental value from Ref. 40.

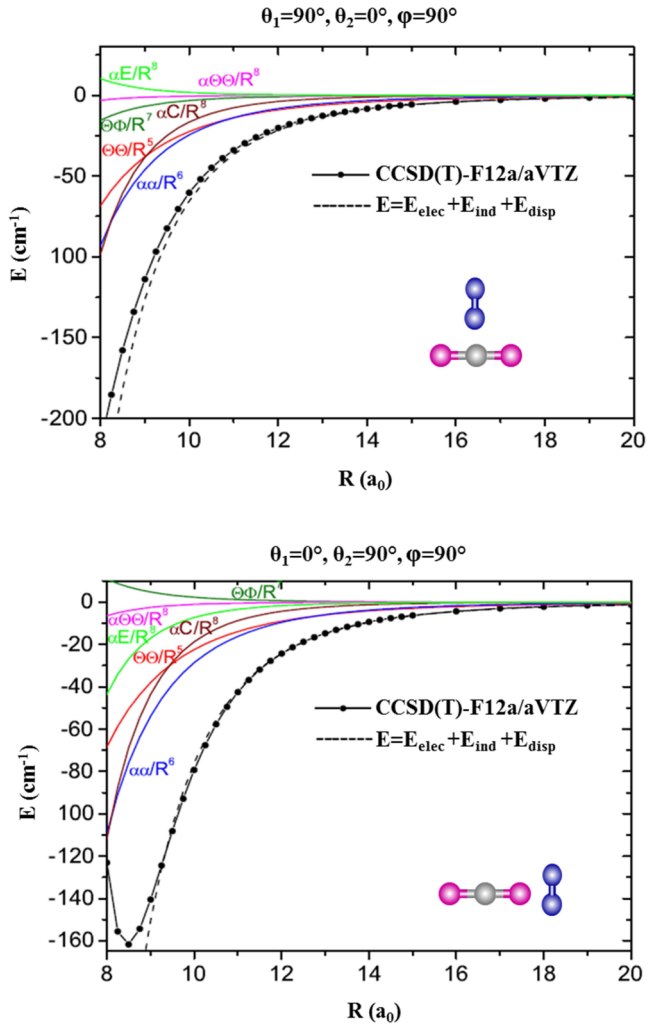

FIG. 2. R-dependence of the potential energy for the two most stable configurations. These curves are computed using CCSD(T)-F12a/aug-cc-pVTZ method and multipolar expansion (Eqs. (1)–(3)).

actions. Therefore, the *ab initio* calculations of the 4D-PES of the CO_2–N_2 complex were carried out at this level of theory. The 4D-PES of the ground state of CO_2–N_2 is mapped along the Jacobi vdW internal coordinates (R, θ_1, θ_2, and φ, Figure 3). R is the distance from the carbon atom to the N_2 center of mass, θ_1 denotes the enclosed angle between the R vector and the molecular axis of CO_2, θ_2 represents the angle between the R vector and the molecular axis of N_2, and φ denotes the dihedral angle between half-planes containing the CO_2 and N_2 bonds. For symmetry reasons, the calculations of the PES were carried out for angle θ_1 ranging from 0° to 180° (with a step of 15°), for angle θ_2 from 0° to 90° (with a step of 15°), and for angle φ from 0° to 90° (with a step of 30°). The grid on R was irregular where it took 60 values in the 4-30 interval (in bohr). In total, the grid of configurations consisted of 21 840 non-equivalent geometries. Here, the monomers were considered as rigid.

Because of the use of scaled F12 triple energy correction within CCSD(T)-F12 as implemented in MOLPRO, the CCSD(T)-F12 method is non-consistent.[22] To correct for this non-consistency, the energies were shifted down by the value of the interaction energy for R = 100 bohr (see Ref. 12 for more details). Nevertheless, this correction is small for the present system (i.e., E = 0.016 668 53 cm^{-1}).

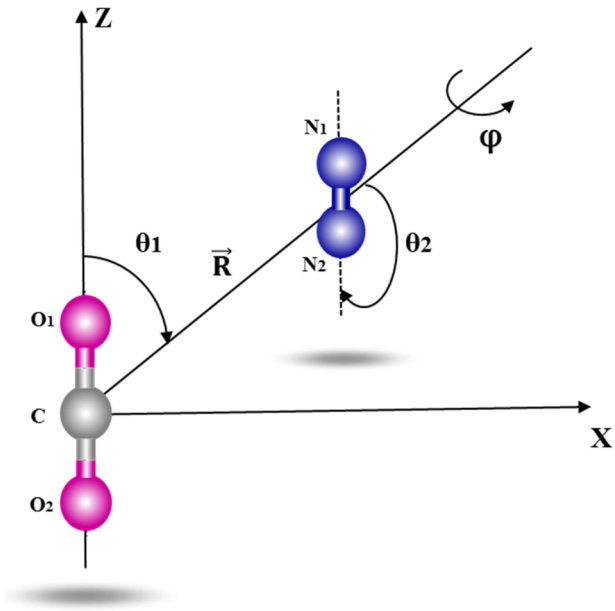

FIG. 3. Definition of the coordinate system for CO_2–N_2.

B. Analytical representation of the PES

The functional form of the 4D-PES is developed on a basis of angular functions

$$V(R,\theta_1,\theta_2,\varphi) = \sum_{l_1=0}^{N_1}\sum_{l_2=0}^{N_2}\sum_{m=0}^{\min(l_1,l_2,N_m)} F^m_{l_1l_2}(R)\bar{P}^m_{l_1}(\cos\theta_1) \times \bar{P}^m_{l_2}(\cos\theta_2)\cos(m\varphi), \quad (4)$$

where $\bar{P}^m_l$ are normalized associated Legendre functions. Both N_2 and CO_2 molecules have a center of symmetry; thus, the sums over l_1 and l_2 are restricted to even values. The expansion is limited to $N_1 = 12$, $N_2 = 12$, $N_m = 6$. For each point of the radial grid, a least-square procedure has been performed to compute the coefficients of the development on the angular functions. Then, the radial functions are obtained by cubic spline interpolation. Outside the range of the radial grid, the radial functions are extrapolated for shorter distances by

$$F^m_{l_1l_2}(R) = \tau^m_{l_1l_2}\exp(-\gamma^m_{l_1l_2}R). \quad (5)$$

The parameters $\tau^m_{l_1l_2}$ and $\gamma^m_{l_1l_2}$ were defined by requiring the continuity of the radial functions and their first derivatives at $R = 4\ a_o$.

The root mean square (RMS) of the error of the fit was monitored for each least-square interpolation performed at each point of the radial grid. The RMS of the error is roughly proportional to the average potential energy at each point of the radial grid. At $R = 6\ a_o$, the RMS of the error is 0.93 cm^{-1}, at $R = 10\ a_o$, it is 0.001 cm^{-1}, and at $R = 15\ a_o$, it is 0.0006 cm^{-1}. The analytical form of the 4D-PES can be sent upon request.

IV. DESCRIPTION OF THE 4D-PES

In the ground PES of CO_2–N_2, four stationary points were found. They are displayed in Figure 4. They correspond to two minimal structures (denoted as MIN1 and MIN2 in

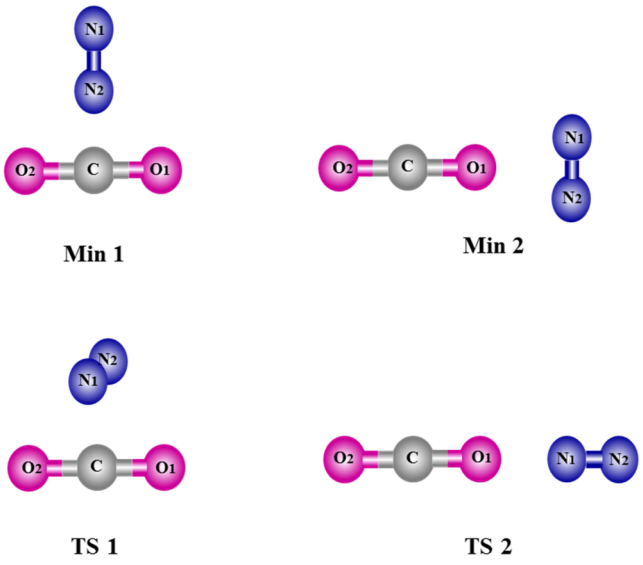

FIG. 4. Stationary points on the ground PES of CO_2–N_2 complex.

Figure 4) and two transition states (TS1 and TS2 in Figure 4). The nature (MIN or TS) of these forms was checked after geometry optimizations in the C_1 point group and frequency computations. These calculations were performed at the CCSD(T)-F12a/aug-cc-pVTZ level and where all coordinates were fully relaxed. The results are listed in Table II. Note that the intramonomer equilibrium distances remain almost unchanged upon complexation. Indeed, Table II shows that the r(CO) and r(NN) in the monomers differ only slightly from those in the CO_2–N_2 complex. This justifies the rigid monomer approximation used at present for the generation of the PES of CO_2–N_2 complex. The main characteristics of these stationary points and their comparison to previous data are given in Table III. Strictly speaking, φ is not defined when θ_1 or θ_2 take the values 0° or 180°. Nevertheless, we will assign a value for the φ angle for consistency with previous works.

The global minimum of the 4D-PES (MIN1) corresponds to a T-shape structure where the nitrogen molecular axes point towards the carbon atom of CO_2: $\theta_1 = 90°$, $\theta_2 = 0°$, $\varphi = 90°$, and R = 6.96 a_0 with a well depth of $D_e = -325.03$ cm^{-1} (MIN1, cf. Figure 4 and Table II). This finding is in good agreement with previous theoretical determinations. Indeed, Table III shows that R value deduced from our 4D-PES is close to the one computed at the CCSD(T)-F12(a/b)/cc-pVXZ-F12 and CCSD(T)/aug-cc-pVXZ levels.[10] Our R value is also in good agreement with those determined experimentally.[5,8] Interestingly, the depth of the potential issued from our 4D-PES is close to depths computed using the cc-pVXZ-F12 basis set in connection with the CC explicitly correlated method. In our recent benchmark investigations of the HCl–He complex,

TABLE II. Spectroscopic parameters of the free monomers and of the CO_2–N_2 complex computed at the CCSD(T)-F12a/aug-cc-pVTZ level of theory, where all degrees of freedom were relaxed. The ω_i (in cm^{-1}) are the harmonic frequencies. Distances are in a_0. D_e is the dissociation energy in cm^{-1}. See Figure 4 for the designation of the considered CO_2–N_2 structures.

		Bond length		
Monomer	Bond	Computed	Experimental[44]	Percentage error
CO_2	r_{CO}	2.1956	2.1960	0.02
N_2	r_{NN}	2.0763	2.0673	0.47
		Frequencies		
Monomer	Mode	Computed	Experimental[45]	Percentage error
CO_2	ω_s (OCO)	1351	1388.17	2.66
	ω_b (OCO)	675	667.40	1.23
	ω_{as} (OCO)	2392	2349.16	1.85
N_2	ω (NN)	2360	2359.61	0.04
		CO_2–N_2		
Frequency	MIN 1	MIN 2	TS1	TS2
ω_{as} (OCO)	2393	2392	2392	2390
ω (NN)	2361	2360	2258	2359
ω_s (OCO)	1351	1351	1350	1350
ω_{oop} (OCO)	676	674	671	675
ω_b (OCO)	673	674	671	674
ω (CNN)	88	44	39	27
ω (CN)	61	42	18	i 15
ω_{oop}	46	17	10	13
$\omega_{torsion}$	32	10	i 35	i 22
r_{CO}	2.1962	2.1960	2.1961	2.1964
r_{NN}	2.0773	2.0777	2.0775	2.0779
R_e	6.96	8.42	6.37	9.87
D_e (cm^{-1})	−325.03	−159.62	−158.55	−26.63

TABLE III. Characteristics of the stationary points of the 4D-PES of CO_2–N_2 and comparison with previous experimental and theoretical works. See Figure 4 for the designation of the considered CO_2–N_2 structures.

	MIN1		MIN2		TS1		TS2	
	$\theta_1 = 90, \theta_2 = 0, \varphi = 90$		$\theta_1 = 0, \theta_2 = 90, \varphi = 90$		$\theta_1 = \theta_2 = \varphi = 90$		$\theta_1 = \theta_2 = 0, \varphi = 90$	
Method/Basis set	R (bohr)	V (cm^{-1})	R (bohr)	V (cm^{-1})	R (bohr)	V (cm^{-1})	R (bohr)	V (cm^{-1})
CCSD(T)-F12a/aug-cc-pVTZ	6.98	−321.24	8.47	−158.90	6.42	−163.58	9.93	−30.56
CCSD(T)-F12a/cc-pVDZ-F12[a]	6.96	−325.27						
CCSD(T)-F12a/cc-pVTZ-F12[a]	6.95	−325.27						
CCSD(T)-F12a/cc-pVQZ-F12[a]	6.95	−328.77						
CCSD(T)-F12b/cc-pVDZ-F12[a]	6.98	−318.28						
CCSD(T)-F12b/cc-pVTZ-F12[a]	6.95	−325.27						
CCSD(T)-F12b/cc-pVQZ-F12[a]	6.95	−325.27						
CCSD(T)/aug-cc-pVDZ[a]	6.92	−458.18						
CCSD(T)/aug-cc-pVTZ[a]	6.92	−388.23						
CCSD(T)/aug-cc-pVQZ[a]	6.93	−360.25						
CCSD(T)/aug-cc-pV5Z[a]	6.94	−335.76						
CCSD(T)/aug-cc-pV6Z[a]	6.94	−332.27						
CCSD(T)/CBS aug-cc-pVDZ/aug-cc-pVTZ[a]		−367.24						
CCSD(T)/CBS aug-cc-pVTZ/aug-cc-pVQZ[a]		−346.26						
CCSD(T)/CBS aug-cc-pVQZ/aug-cc-pV5Z[a]		−318.28						
CCSD(T)/CBS aug-cc-pV5Z/aug-cc-pV6Z[a]	6.94	−328.77						
CCSD(T)/aug-cc-pVQZ[b]	7.16	−316.70	8.61	−152.30	6.51	−152.50		
CCSD(T)/CBS[b]		−317.00						
CCSD(T)/CBS (+MB)[b,c]		−321.30						
CCSD(T)/final CBS[b,d]		−319.20						
MP4/aug-cc-pVQZ[b]	6.95	−348.20	8.44	−169.50	6.46	−170.20		
MP4/CBS[b]		−349.90						
MP4/CBS (+MB)[b,c]		−353.10						
MP4/final CBS[b,d]		−351.50						
MP2/aug-cc-pVDZ[e]		−290.30						
MP2/aug-cc-pVTZ[f]	6.99	−322.82						
MP2/6-311+G(d)[g]	7.09	−205.891						
Exp1[h]	7.04	−453.00	8.20	−239.00		−284.00		
Exp2[i]	7.04							

[a]All calculations were carried out at the CCSD(T)-F12b/cc-VQZ-F12 optimized geometry.[10]
[b]Interaction energies were extrapolated to the CBS limit[11] by a procedure based on the formula proposed by Helgaker *et al.*[46,47]
[c]Basis set extended by 3s3p2d1f1g midbond functions (MB) centered in the middle of the intermolecular bond.[11]
[d]The final CBS limit is taken as an arithmetic mean of the CBS and CBS (+MB) limit extrapolated using the aug-cc-pVXZ and aug-cc-pVXZ + MB basis set (X = D, T).[11]
[e]Reference 6.
[f]Reference 7.
[g]Reference 9.
[h]Results obtained from infrared spectrum in the region of the ν_3 asymmetric stretch of CO_2 monomer Ref. 5.
[i]Reference 8. The geometrical parameters of the T-shaped ground-state structure are determined from 90 - $\theta_{NcmCO} = 6.85°(3)$ which represents root mean square of the angle deviation angle where θ_{NcmCO} is the angle $N_{cm}-C-O$ (cm is the center of mass in N_2 subunit).[8]

we showed, however, some deficiencies of these basis sets for the description of weakly bound complexes.[15] The main difference between CO_2–N_2 and HCl–He is that the bonding in CO_2–N_2 is much stronger than in HCl–He resulting in a potential well ten times larger for CO_2–N_2. At present, we may state that the use of cc-pVXZ-F12 basis sets in connection with CCSD(T)-F12 methodologies is possible for relatively strong vdW systems. Their application should not be considered as straightforward. Moreover, Table III shows that the present dissociation energy is off by ∼30% from the experimental value of Walsh *et al.*[5] This deviation may be related to the fact that the experiments were performed at ν_3 asymmetric stretch of CO_2 rather than the ground state. Indeed, this induces changes on the shape of the PES and hence on dissociation energies. Similar deviations were noticed recently for the CO_2–CO_2 complex.[17]

MIN2 corresponds to a T-shape structure where one O atom of CO_2 molecule points towards the center of mass of N_2. It is located at $\theta_1 = 0°$, $\theta_2 = 90°$, $\varphi = 90°$, R = 8.42 a_0. This isomer is also of C_{2v} symmetry. The depth of the potential well associated with MIN2 is $D_e = -159.62$ cm^{-1}. MIN2 was already identified through the MP4 and CCSD(T) investigations by Fišer *et al.*[11] and after the analysis of the IR spectrum of CO_2–N_2 in the region of the ν_3 asymmetric stretch of CO_2 monomer.[5]

TS1 is located close in energy to MIN2 and possesses crossed form (i.e., $\theta_1 = 90°$, $\theta_2 = 90°$, $\varphi = 90°$, and R = 6.37 a_0). TS1 was identified in Ref. 5 to be a minimal structure. Instead, our work shows that it is a transition state that connects the two equivalent forms of MIN1 after inversion of the N_2 moiety. Fišer *et al.*[11] characterized also this TS. In addition, we locate a linear transition state (TS2) at relatively large

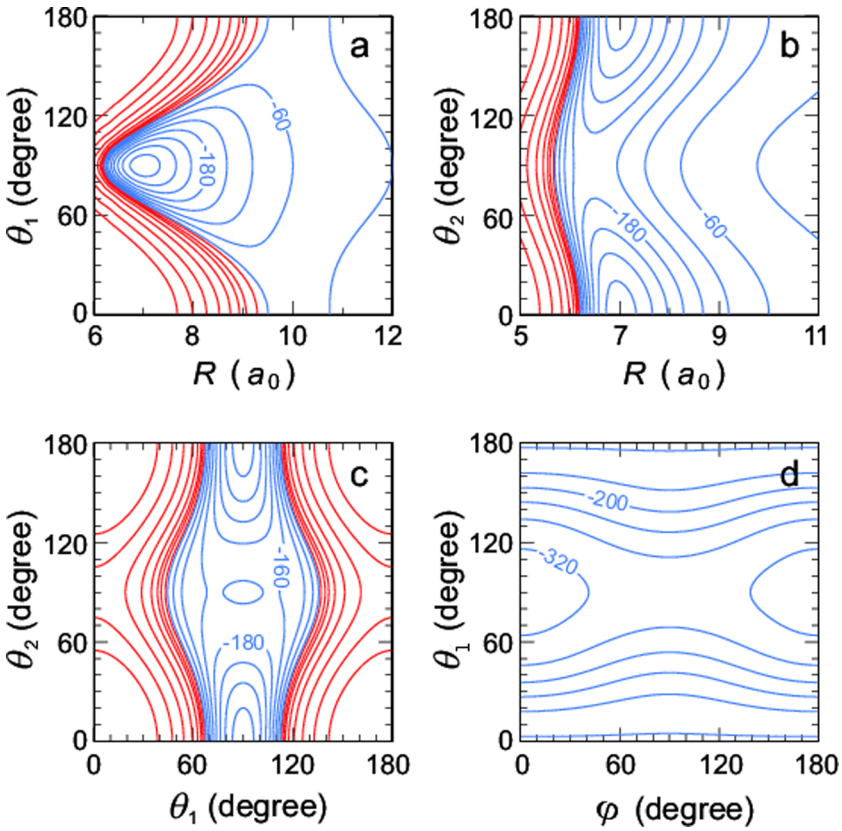

FIG. 5. Contour plots of the interaction energy. (a) $\theta_2 = 0°$; (b) $\theta_1 = 90$, $\varphi = 90°$; (c) R = 6.98 a_0, $\varphi = 90°$; (d) R = 6.98 a_0, $\theta_2 = 0°$. Negative contour lines (blue) are equally spaced by 40 cm^{-1}. The zero energy contour line is red and the next red energy contour line is at 40 cm^{-1}. The energy is multiplied by 2 for each next red contour lines.

internuclear distances ($\theta_1 = 0°$, $\theta_2 = 0°$, $\varphi = 90°$ and R = 9.87 a_0). It is lying at 30 cm^{-1} below the $CO_2 + N_2$ dissociation limit. TS2 has never been found previously. TS2 connects the two MIN2 equivalent minima. Note that both TS1 and TS2 are located below the $CO_2 + N_2$ dissociation limit. The inversions of N_2 within MIN1 were already noticed in the literature, whereas we point out the large amplitude motions exhibited by N_2 within MIN2 for the first time.

Figure 5 depicts the bi-dimensional cuts of the 4D-PES of CO_2–N_2 along two Jacobi coordinates where the other coordinates were set at their equilibrium values in MIN1. The two stable structures and the two transition states can be easily identified in the minima and the extrema of the PES, respectively. Moreover, this figure shows that the interaction potential between CO_2 and N_2 is strongly anisotropic and that the internal bending motion and the intermonomer motions are coupled mutually. Strong anharmonic resonances are expected to occur. In addition, the parts of the 4D-PES are flat along these coordinates. This is related to the weakly bound nature of the CO_2–N_2 dimer. Consequently, we expect a high density of rovibrational levels for this complex composed by second raw elements. Large amplitude motions are also likely to take place. Such characteristics are common for van der Waals complexes.

Figure 6 displays the one-dimensional evolution of the interaction potential vs. the θ_1 bending coordinate for different values of θ_2 angles. For $\theta_2 = 0°$, a unique minimum is found, whereas the potential exhibits three minima when θ_2 is larger than ~10°. The triple well potential is symmetric with respect to the $\theta_1 = 90°$ configuration. This shape of the PES along the θ_1 coordinate is close to the one predicted using semi-empirical considerations by Walsh *et al.* (cf. Figure 5 of Ref. 5). Indeed, these authors established that this triple well is due to the sum of the distributed multipole potential and the distributed isotropic dispersion interaction contributions. More interestingly, this special shape induces "an artificial non-symmetric equilibrium structure" for MIN1 when the rovibrational levels are populated as noticed by Frohman *et al.*[7] Indeed, these authors showed that the N≡N axis makes an angle of ~19.2° with the C_2 axis of the complex. For that purpose, they used the relation connecting this angle and the ratio between the experimental nuclear quadrupole coupling constant of nitrogen in the complex and the value of the nuclear quadrupole coupling constant of ^{14}N in free molecular N_2.

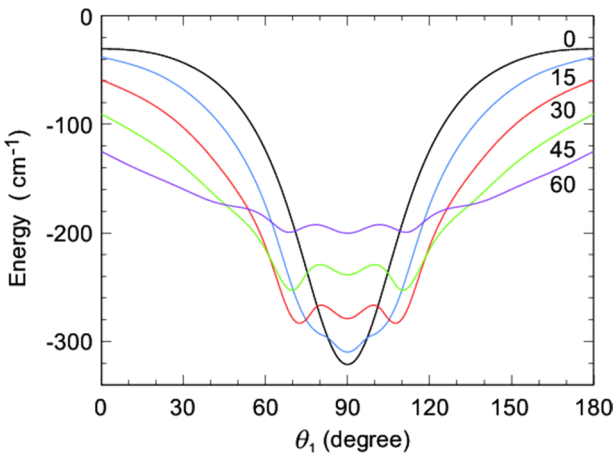

FIG. 6. Selected one-dimensional cuts of the interaction energy with φ and R relaxed. The value of θ_2 is indicated for each curve.

Then, this r_0 structure served to assign their $^{12}C^{16}O_2$–$^{14}N_2$ μw spectrum. After considering the zero point vibrational energy correction (~20 cm^{-1}), we estimate a θ_2 angle of ~20° for the r_0 structure of CO_2–N_2, which is in excellent agreement with the empirical findings of Frohman *et al.*[7] For $^{12}C^{18}O_2$–$^{14}N_2$, the θ_2 deviation from the C_{2v} equilibrium structure is estimated to be ~6.8° through the analysis of the infrared diode laser spectrum of this isotopologue.[8] The larger θ_2 and r_0 values for ^{16}O complex with respect to ^{18}O complex are in line with the smaller zero point energy (ZPE) for the heavier one and therefore on the location of the corresponding vibrationless level on the PES relative to the global minimum.

V. CONCLUSIONS

Using an explicitly correlated methodology, we generated the 4D-PES of the CO_2–N_2 dimer along the intermonomer Jacobi coordinates. This PES is strongly anharmonic where two minimal structures and two transition states were located. Both minimal structures at equilibrium (i.e., r_e structures) are of C_{2v} symmetry, whereas the experimentally observed deviations from these structures are rationalized in terms of r_0 structures when ZPE correction is taken into account. Moreover, we confirm the occurrence of large amplitude motions, namely, the N_2 inversion within MIN1 as stated previously. Also, we expect that N_2 does such large amplitude motion within MIN2. TS1 and TS2 are the transition states connecting both equivalent corresponding minima.

These interesting and specific PES features should result on unusual pattern of rovibrational levels for CO_2–N_2. We plan to present such spectrum, which is obtained using quantum molecular dynamics based on our highly accurate 4D PES. We plan also to deduce the cross sections for the CO_2 (de-)excitation in collisions with N_2.

ACKNOWLEDGMENTS

We acknowledge the financial support through a Marie Curie International Research Staff Exchange Scheme Fellowship within the 7th European Community Framework Program under Grant No. PIRSES-GA-2012–317544 and the COST Action CM1405 MOLIM. Y.K. greatly acknowledges the financial support of RFBR Grants, 13-05-00751 and 15-05-00736. Y.K. acknowledges Tomsk State University Competitiveness Improvement Program.

[1]Y. Xu and W. Jager, J. Mol. Struct. **599**, 211-217 (2001).
[2]J. M. Hutson, A. Ernesti, M. M. Law, C. F. Roche, and R. J Wheatley, J. Chem. Phys. **105**, 9130 (1996).
[3]R. Chen, H. Zhu, and D. Xie, Chem. Phys. Lett. **511**, 229-234 (2011).
[4]H. Li, P.-N. Roy, and R. J. Le Roy, J. Chem. Phys. **132**, 214309 (2010).
[5]M. A. Walsh, T. R. Dyke, and B. J. Howard, J. Mol. Struct. **189**, 111-120 (1988).
[6]J. A. Gomez Castano, A. Fantoni, and R. M. Romano, J. Mol. Struct. **881**, 68-75 (2008).
[7]D. J. Frohman, E. S. Contreras, R. S. Firestone, S. E. Novick, and W. Klemperer, J. Chem. Phys. **133**, 244303 (2010).
[8]T. Konno, S. Yamaguchi, and Y. Ozaki, J. Mol. Spectrosc. **270**, 66-69 (2011).
[9]M. Venayagamoorthy and T. A. Ford, J. Mol. Struct. **565-566**, 399-409 (2001).
[10]K. M. de Lange and J. R. Lane, J. Chem. Phys. **134**, 034301 (2011).
[11]J. Fišer, T. Boublík, and R. Polák, Collect. Czech. Chem. Commun. **69**, 177 (2004).
[12]F. Lique, J. Klos, and M. Hochlaf, Phys. Chem. Chem. Phys. **12**, 15672 (2010).
[13]P. Halvick, T. Stoecklin, F. Lique, and M. Hochlaf, J. Chem. Phys. **135**, 044312 (2011).
[14]K. Mathivon, R. Linguerri, and M. Hochlaf, J. Chem. Phys. **139**, 164306 (2013).
[15]Y. Ajili, K. Hammami, N. E. Jaidane, M. Lanza, Y. N. Kalugina, F. Lique, and M. Hochlaf, Phys. Chem. Chem. Phys. **15**, 10062 (2013).
[16]M. Mogren Al Mogren, O. Denis-Alpizar, D. Ben Abdallah, T. Stoecklin, P. Halvick, M.-L. Senent, and M. Hochlaf, J. Chem. Phys. **141**, 044308 (2014).
[17]Y. N. Kalugina, I. A. Buryak, Y. Ajili, A. A. Vigasin, N. Jaidane, and M. Hochlaf, J. Chem. Phys. **140**, 234310 (2014).
[18]H.-J. Werner, P. J. Knowles, G. Knizia, F. R. Manby, M. Schütz *et al.*, MOLPRO, version 2012.1, a package of *ab initio* programs, 2012, see http://www.molpro.net.
[19]S. F. Boys and F. Bernardi, Mol. Phys. **19**, 553 (1970).
[20]P. J. Knowles, C. Hampel, and H.-J. Werner, J. Chem. Phys. **99**, 5219 (1993).
[21]P. J. Knowles, C. Hampel, and H.-J. Werner, J. Chem. Phys. **112**, E3106 (2000).
[22]G. Knizia, T. B. Adler, and H. Werner, J. Chem. Phys. **130**, 054104 (2009).
[23]K. A. Peterson, D. E. Woon, and T. H. Dunning, Jr., J. Chem. Phys. **100**, 7410 (1994).
[24]D. Feller and J. A. Sordo, J. Chem. Phys. **112**, 5604 (2000).
[25]T. H. Dunning, Jr., J. Chem. Phys. **90**, 1007 (1989).
[26]R. A. Kendall, T. H. Dunning, Jr., and R. J. Harrison, J. Chem. Phys. **96**, 6796 (1992).
[27]W. Klopper, Mol. Phys. **99**, 481 (2001).
[28]F. Weigend, A. Kohn, and C. Hattig, J. Chem. Phys. **116**, 3175 (2002).
[29]See supplementary material at http://dx.doi.org/10.1063/1.4919396 for the imaginary frequency dependent polarizabilities (independent components) for N_2 and CO_2 molecules and for characteristics of a single point calculation of the interaction energy of CO_2-N_2 complex.
[30]A. D. Buckingham, in *Intermolecular Interactions: From Diatomics to Biopolymers*, edited by B. Pullman (Wiley, 1978).
[31]H. Kling and W. Huettner, Chem. Phys. **90**, 207 (1984).
[32]J. N. Watson, I. E. Craven, and G. L. D. Ritchie, Chem. Phys. Lett. **274**, 1 (1997).
[33]G. Maroulis, Chem. Phys. **291**, 81 (2003).
[34]A. Chrissanthopoulos, U. Hohm, and U. Wachsmuth, J. Mol. Struct. **526**, 323 (2000).
[35]C. Graham, D. A. Imrie, and R. E. Raab, Mol. Phys. **93**, 49 (1998).
[36]G. Maroulis, J. Chem. Phys. **118**, 2673 (2003).
[37]A. D. Buckingham, C. Graham, and J. H. Williams, Mol. Phys. **49**, 703 (1983).
[38]M. Bartolomei, E. Carmona-Novillo, M. I. Hernandez, J. Campos-Martinez, and R. Hernandez-Lamoneda, J. Comput. Chem. **32**, 279 (2010).
[39]N. J. Bridge and A. D. Buckingham, Proc. R. Soc. London, Ser. A **295**, 334 (1966).
[40]A. Kumar and W. J. Meath, Theor. Chim. Acta **82**, 131 (1992).
[41]H. D. Cohen and C. C. J. Roothaan, J. Chem. Phys. **43**, S34 (1965).
[42]T. Korona, M. Przybytek, and B. Jeziorski, Mol. Phys. **104**, 2306 (2006).
[43]O. Denis-Alpizar, Y. Kalugina, T. Stoecklin, M. H. Vera, and F. Lique, J. Chem. Phys. **139**, 224301 (2013).
[44]G. Herzberg, *Molecular Spectra and Molecular Structure*, Electronic Spectra and Electronic Structure of Polyatomic Molecules Vol. III (Van Nostrand, Princeton, NJ, 1966).
[45]K. P. Huber and G. Herzberg, *Molecular Spectra and Molecular Structure*, Constants of Diatomic Molecules Vol. IV (Van Nostrand Reinhold, Wokingham, 1979).
[46]T. Helgaker, W. Klopper, H. Koch, and J. Noga, J. Chem. Phys. **106**, 9639 (1997).
[47]A. Halkier, T. Helgaker, P. Jørgensen, W. Klopper, H. Koch, J. Olsen, and A. K. Wilson, Chem. Phys. Lett. **286**, 243 (1998).